Biochemical and Biophysical Research Communications 457 (2015) 50–57

Contents lists available at ScienceDirect

Biochemical and Biophysical Research Communications

journal homepage: www.elsevier.com/locate/ybbrc

Different conformational dynamics of β-arrestin1 and β-arrestin2 analyzed by hydrogen/deuterium exchange mass spectrometry

Youngjoo Yun [a,1], Dong Kyun Kim [a,1], Min-Duk Seo [b], Kyeong-Man Kim [c], Ka Young Chung [a,*]

[a] School of Pharmacy, Sungkyunkwan University, Suwon, Republic of Korea
[b] College of Pharmacy & Department of Molecular Science and Technology, Ajou University, Suwon, Republic of Korea
[c] College of Pharmacy, Chonnam National University, Gwang-Ju, Republic of Korea

ARTICLE INFO

Article history:
Received 6 December 2014
Available online 23 December 2014

Keywords:
β-Arrestin
Pre-activation
Conformational dynamics
Hydrogen/deuterium exchange mass spectrometry

ABSTRACT

Arrestins have important roles in G protein-coupled receptor (GPCR) signaling including desensitization of GPCRs and G protein-independent signaling. There have been four arrestins identified: arrestin1, arrestin2 (e.g. β-arrestin1), arrestin3 (e.g. β-arrestin2), and arrestin4. β-Arrestin1 and β-arrestin2 are ubiquitously expressed and regulate a broad range of GPCRs, while arrestin1 and arrestin4 are expressed in the visual system. Although the functions of β-arrestin1 and β-arrestin2 widely overlap, β-arrestin2 has broader receptor selectivity, and a few studies have suggested that β-arrestin1 and β-arrestin2 have distinct cellular functions. Here, we compared the conformational dynamics of β-arrestin1 and β-arrestin2 by hydrogen/deuterium exchange mass spectrometry (HDX-MS). We also used the R169E mutant as a pre-activation model system. HDX-MS data revealed that β-strands II through IV were more dynamic in β-arrestin2 in the basal state, while the middle loop was more dynamic in β-arrestin1. With pre-activation, both β-arrestin1 and β-arrestin2 became more flexible, but broader regions of β-arrestin1 became flexible compared to β-arrestin2. The conformational differences between β-arrestin1 and β-arrestin2 in both the basal and pre-activated states might determine their different receptor selectivities and different cellular functions.

1. Introduction

Arrestins are a family of four homologous proteins that have important regulating roles in G protein-coupled receptor (GPCR) signaling [1]. The four homologs are arrestin1 (e.g. visual arrestin or S-arrestin), arrestin2 (e.g. β-arrestin1), arrestin3 (e.g. β-arrestin2), and arrestin4 (e.g. cone arrestin or X-arrestin) [1]. Arrestin1, the first discovered arrestin in the visual system, was found to desensitize rhodopsin signaling by interacting and internalizing phosphorylated light-activated rhodopsin [2]. Later, two non-visual ubiquitously expressed arrestins, β-arrestin1 and β-arrestin2, were found to regulate internalization and desensitization of various non-rhodopsin GPCRs including the β2-adrenergic receptor [1,3–6]. Recent studies suggest that arrestins are involved not only in GPCR desensitization but also in G protein-independent signaling [1].

β-Arrestin1 and β-arrestin2 are 75% identical by amino acid sequence and 85% similar accounting for conservative substitutions [1] (Fig. 1A). Knock-outs of either β-arrestin1 or β-arrestin2 produce grossly normal mice, while a knock-out of both β-arrestins is embryonically lethal [7], which suggests that β-arrestins are functionally redundant. Although the function of β-arrestin1 and β-arrestin2 widely overlap, their affinity for GPCRs has been shown to be different [8]. Oakley et al. classified GPCRs based on their affinity for arrestins; class A GPCRs bind β-arrestin2 with higher affinity than β-arrestin1, whereas class B GPCRs bind β-arrestin1 and β-arrestin2 with similar high affinities, which implies that β-arrestin2 has a wider receptor selectivity [1,8,9]. Besides receptor selectivity, β-arrestin1 and β-arrestin2 have different cellular functions [10–13]. There are more than 30 arrestin-binding partners including adaptor proteins and MAP kinases, and the different binding capabilities between β-arrestin1 and β-arrestin2 may result in different cellular functions [14,15].

Few studies including X-ray crystallography, limited tryptic proteolysis, and DEER spectroscopy have reported conformational differences between β-arrestin1 and β-arrestin2 [16–19]. However, conformational differences between β-arrestin1 and β-arrestin2 in the basal and active states are not yet fully understood. The present study compared the conformations of β-arrestin1 and β-arrestin2 by hydrogen/deuterium exchange mass spectrometry (HDX-MS). Mutation of Arg169 to Glu (R169E

* Corresponding author at: 2066 Seobu-ro, Jangan-gu, Suwon 440-746, Republic of Korea. Fax: +82 31 292 8800.
E-mail address: kychung2@skku.edu (K.Y. Chung).
[1] These authors contributed equally to this work.

http://dx.doi.org/10.1016/j.bbrc.2014.12.079
0006-291X/

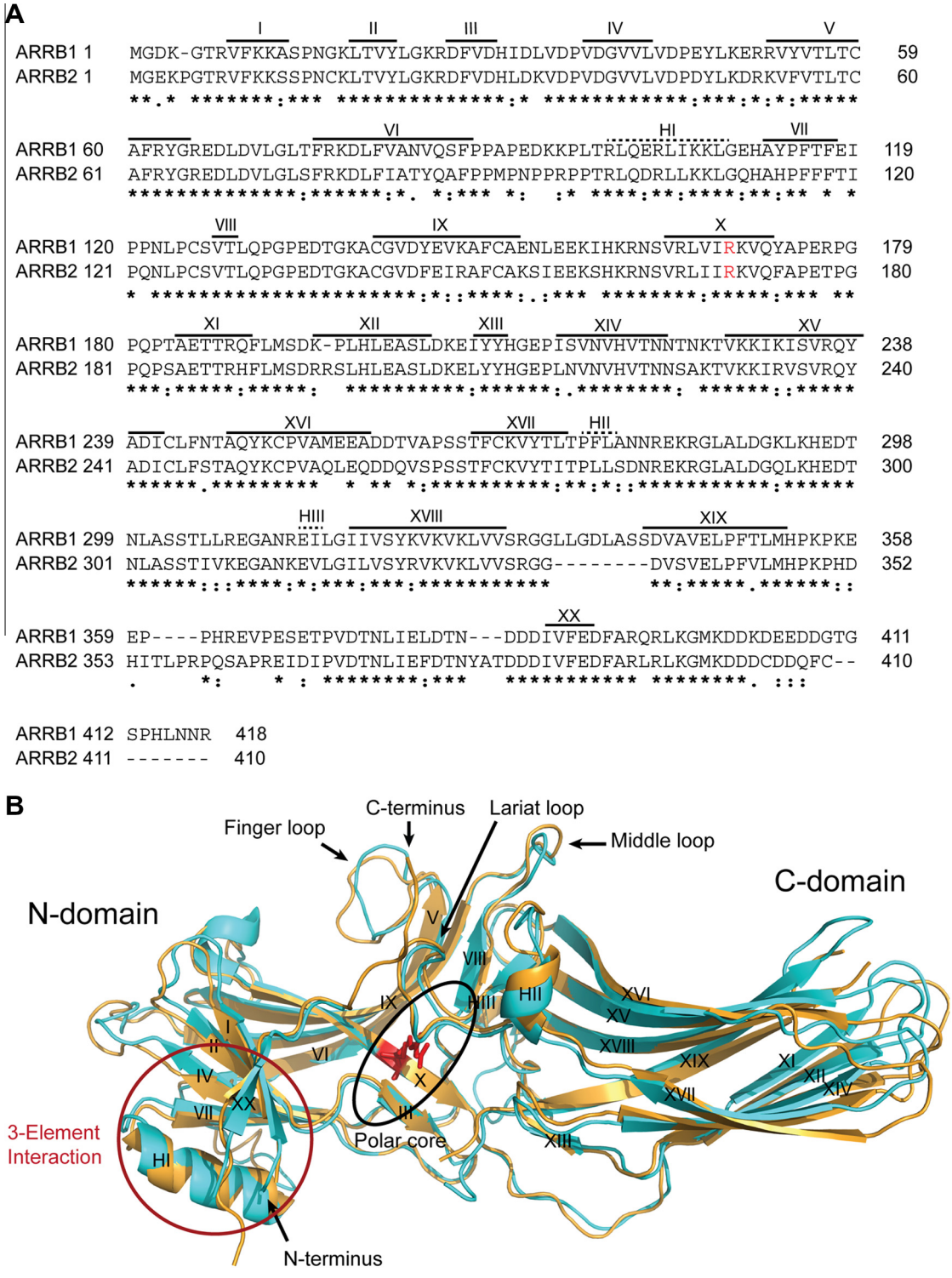

Fig. 1. Sequence and structure alignment of β-arrestin1 and β-arrestin2. (A) Sequence alignment of rat β-arrestin1 and rat β-arrestin2. β-Strands and α-helices are indicated as solid or dotted lines above the sequence alignment. The arginine involved in salt bridge formation in the polar core is colored red. (B) Structure alignment of β-arrestin1 and β-arrestin2. High resolution structures were adopted from X-ray crystal structures of β-arrestin1 (orange, PDB: 1JSY) and β-arrestin2 (light blue, PDB: 3P2D). The arginine involved in salt bridge formation in the polar core is shown as a red stick. (For interpretation of the references to colour in this figure legend, the reader is referred to the web version of this article.)

mutant) in β-arrestin1 (Arg170 in β-arrestin2) resulted in arrestins that bound to activated GPCRs in a phosphorylation-independent manner [20,21]. Using this mutant as a pre-activated conformation of β-arrestins, we analyzed the conformational dynamics of the basal and pre-activated states of β-arrestin1 and β-arrestin2.

2. Material and methods

2.1. Materials

Unless otherwise noted, all materials were purchased from Sigma–Aldrich (St Louis, MO). DNaseI was obtained from Roche

(Basel, Switzerland); the protease inhibitor cocktail was obtained from Merck Millipore (Billerica, MA, USA); leupeptin was obtained from Calbiochem (San Diego, CA, USA); glutathione-superflow resin was obtained from Clontech (Mountain View, CA, USA); deuterium oxide was obtained from Cambridge Isotope Laboratories (Tewksbury, MA, USA); isopropyl-thio-β-D-galactopyranoside (IPTG) was obtained from Noble Bio (Hwaseong, Republic of Korea).

2.2. Expression of β-arrestin1 and β-arrestin2

cDNAs of rat wild type β-arrestin1 and rat wild type β-arrestin2 were a generous gift from professor Kyeong-Man Kim, and R169E mutants were generated by site-directed mutagenesis using PCR. The coding sequences of wild type and R169E of β-arrestin1 and β-arrestin2 were inserted into pET28a vectors, which were transformed into E. coli BL21 (DE3). The bacterial cells were grown in terrific broth (TB) medium at 37 °C until the OD_{600} became 0.4–0.6, and protein expression was induced with 0.1 mM IPTG for 4 h at 37 °C for wild type β-arrestin1 and β-arrestin2, for 6 h at 28 °C for β-arrestin1 R169E, and for 24 h at 16 °C for β-arrestin2 R169E. The bacterial cells were harvested and stored at −80 °C.

2.3. Purification of β-arrestin1 and β-arrestin2

The harvest bacterial cell pellets were lysed in lysis buffer (20 mM Tris, 500 mM NaCl, pH 7.4, 10 μg/mL benzamidine, 2.5 μg/mL leupeptin, 5 mg/mL lysozyme) for 30 min at room temperature followed by another 30 min incubation with 10 μg/mL DNaseI. The supernatant was collected by centrifugation at 13,000g for 10 min at 4 °C. Supernatant supplemented with 20 mM imidazole was applied to a Ni–NTA agarose column equilibrated with wash buffer (20 mM Tris, 500 mM NaCl, pH 7.4, 20 mM imidazole, 1 μg/mL protease inhibitor cocktail, 10 μg/mL benzamidine, 2.5 μg/mL leupeptin, 100 μM TCEP). After extensive washing, the bound proteins were eluted with elution buffer (20 mM HEPES, 150 mM NaCl, pH 7.4, 400 mM imidazole, 1 μg/mL protease inhibitor cocktail, 10 μg/mL benzamidine, 2.5 μg/mL leupeptin, 100 μM TCEP). The Ni–NTA-purified protein was loaded onto a Superdex 200 column using an AKTA FPLC (GE Healthcare) for gel filtration, and the β-arrestin protein fractions were separated and collected using separation buffer (20 mM HEPES, 150 mM NaCl, pH 7.4).

2.4. HDX-MS

Purified protein was diluted to 60–100 pmol/μL (60–100 μM) in a buffer composed of 20 mM HEPES and 150 mM NaCl (pH 7.4). Hydrogen/deuterium exchange was initiated by mixing 2 μL of protein with 28 μL of D_2O buffer (20 mM HEPES, pD 7.4, 150 mM NaCl in D_2O), and the mixture was incubated for various time intervals (10, 100, 1000 and 10,000 s) on ice. At the indicated time points, the mixture was quenched by adding 30 μL of ice-cold quench buffer (100 mM NaH_2PO_4, pH 2.01). For non-deuterated (ND) samples, 2 μL of purified protein was mixed with 28 μL of H_2O buffer (20 mM HEPES, pH 7.4, 150 mM NaCl in H_2O), and 30 μL of ice-cold quench buffer was added. Quenched samples were digested online by passing them through an immobilized pepsin column (2.1 × 30 mm) (Life Technologies, Carlsbad, CA, USA) at a flow rate of 100 μL/min with 0.05% formic acid in H_2O at 11 °C. Peptide fragments were subsequently collected on a C18 VanGuard trap column (1.7 μm × 30 mm) (Waters, Milford, MA, USA) for desalting with 0.05% formic acid in H_2O and were then separated by ultra-pressure liquid chromatography using an Acquity UPLC C18 column (1.7 μm, 1.0 × 100 mm) (Waters) at a flow rate of 35 μL/min with an acetonitrile gradient starting with 8% B and increasing to 85% B over 8.5 min. Mobile phase A was 0.1% formic acid in H_2O, and solvent B was acetonitrile containing 0.1% formic acid. To minimize the back-exchange of deuterium to hydrogen, the sample, solvents, trap, and UPLC column were all maintained at pH 2.5 and 0.5 °C during the analysis. Mass spectral analyses were performed with a Xevo G2 Qtof equipped with a standard ESI source (Waters). Mass spectra were acquired in the range of m/z 100–2000 for 12 min in positive ion mode.

2.5. Peptide identification and HDX-MS data processing

Peptic peptides were identified in non-deuterated samples with ProteinLynx Global Server 2.4 (Waters). Searches were run with the variable methionine oxidation modification. To process HDX-MS data, the amount of deuterium in each peptide was determined by measuring the centroid of the isotopic distribution using the DynamX program (Waters). Back-exchange was not corrected because the data consisted of comparisons between β-arrestin1 and β-arrestin2 or between wild type and R169E mutants. All of the data was derived from at least three independent experiments.

3. Results and discussion

3.1. HDX-MS study for basal state β-arrestin1 and β-arrestin2

A few studies have proposed conformational differences between β-arrestin1 and β-arrestin2. X-ray crystal structures of basal β-arrestin1 and β-arrestin2 revealed a conserved arrestin fold with two seven-stranded β sandwiches (e.g. N-terminal and C-terminal domains) (Fig. 1B), but the C-domain β sandwich was more flexible in β-arrestin2 [16,17]. Limited tryptic proteolysis showed different active conformations between β-arrestin1 and β-arrestin2 [19], and DEER spectroscopy suggested that the C-terminal tail is in a different position between receptor-bound β-arrestin1 and receptor-bound β-arrestin2 [18]. However, the conformational differences between β-arrestin1 and β-arrestin2 have not yet been fully elucidated.

We employed HDX-MS to compare the conformation and structural dynamics between β-arrestin1 and β-arrestin2. HDX-MS measures the exchange rate of a peptide amide hydrogen with deuterium in solvent [22]. Exposed or highly dynamic regions show rapid exchange rates while excluded and rigid regions exhibit slow exchange rates [22]. Mass spectrometric identification of peptic peptides from β-arrestin1 and β-arrestin2 resulted in approximately 79% and 90% sequence coverage, respectively (Fig. 2). The deuterium uptake levels of β-arrestin1 and β-arrestin2 are presented as heat maps and are color coded on the X-ray crystal structures (PDB ID: 1JSY for β-arrestin1, PDB ID: 3P2D for β-arrestin2) (Fig. 3A and B). Overall, deuterium uptake levels were relatively lower in the core or ordered regions than in exposed or flexible regions (Fig. 3A and B).

3.2. Comparison of conformational dynamics between basal state β-arrestin1 and β-arrestin2

For a more precise comparison of the conformational dynamics between basal state β-arrestin1 and β-arrestin2, the differences of deuterium uptake levels of wild type β-arrestin1 and β-arrestin2 are presented (Fig. 3C, line graph). Each line indicates average deuterium uptake level differences between β-arrestin1 and β-arrestin2 for exchange durations of 10, 100, 1000, and 10,000 s, which were obtained by subtracting the deuterium uptake levels of β-arrestin1 from those of β-arrestin2. The subtraction was performed based on the sequence alignment in Fig. 1A and the heat maps of three independent experiments. Only regions covered by all three

Fig. 2. Sequence coverage maps of β-arrestin1 (A) and β-arrestin2 (B). Bars indicate identified peptic peptides that were used for heat map generation in Figs. 3 and 4.

independent experiments are presented. Many regions show plus or minus values suggesting different deuterium uptake levels between β-arrestin1 and β-arrestin2 (Fig. 3C, line graph). However, this result might not necessarily represent conformational differences. Neighboring peptides affect the intrinsic hydrogen/deuterium exchange rates of amide hydrogens in a protein [23]. To avoid misinterpretation caused by different intrinsic exchange rates, the intrinsic exchange rates of all amide hydrogens in β-arrestin1 and β-arrestin2 were calculated using software developed by Englander's group (http://hx2.med.upenn.edu/download.html) [23,24]. Differences of the intrinsic exchange rates between β-arrestin1 and β-arrestin2 were determined by subtracting the calculated intrinsic exchange rates of β-arrestin1 from those of β-arrestin2 (Fig. 3C, bar graph). In many regions, the deuterium uptake level difference was in agreement with the intrinsic exchange rate difference, but several regions showed dissimilar trends (e.g. regions marked with dotted lines) (Fig. 3C). β-Strands II through IV showed statistically higher deuterium uptake levels in β-arrestin2, and the middle loop showed statistically higher deuterium uptake levels in β-arrestin1, although the calculated intrinsic exchange rates between β-arrestin1 and β-arrestin2 were similar in these regions (Fig. 3C and D). These results suggest that

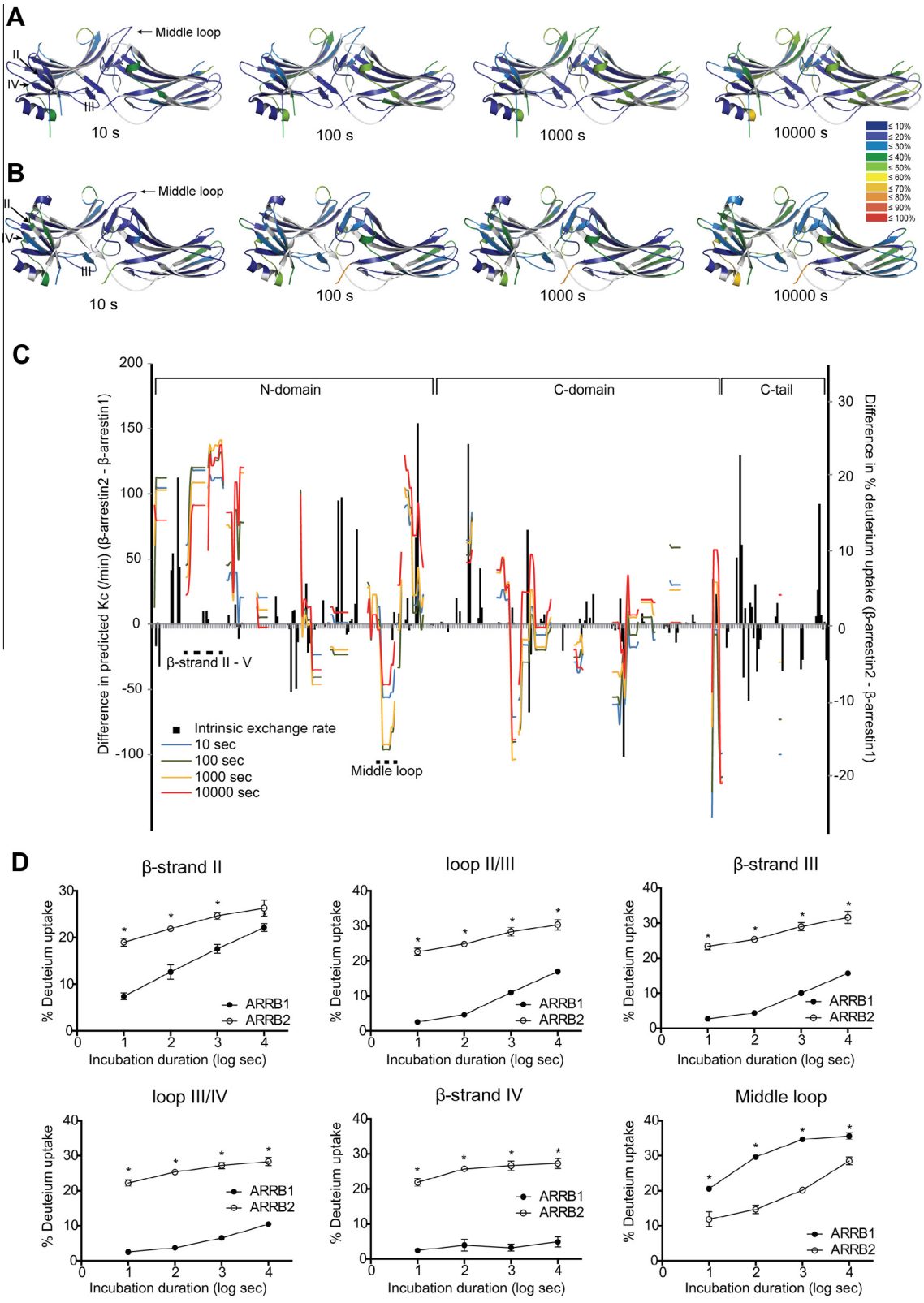

Fig. 3. Comparison of HDX-MS data of β-arrestin1 and β-arrestin2. (A and B) The deuterium uptake profiles were overlaid onto the X-ray crystal structures of β-arrestin1 (A, PDB: 1JSY) and β-arrestin2 (B, PDB: 3P2D). Incorporation of deuterium during 10, 100, 1000 and 10,000 s D_2O buffer incubation is indicated by color code. The color legend shows the deuterium uptake level. Uncovered regions are colored grey. (C) Comparison between the intrinsic exchange rate difference and deuterium uptake level difference. The differences between the calculated intrinsic amide hydrogen/deuterium exchange rates of β-arrestin1 and β-arrestin2 are plotted as a bar graph. The differences between the measured deuterium uptake levels of β-arrestin1 and β-arrestin2 are plotted as line graphs. Deuterium uptake levels for each amide hydrogen are from heat maps of three independent experiments. The *X*-axis is an amino acid sequence number from the N-terminus to C-terminus; several regions are omitted either in β-arrestin1 or β-arrestin2 based on the sequence alignment (Fig. 1A), and those regions are not included. (D) Statistical analysis of deuterium uptake level differences. Deuterium uptake levels in the dotted regions in Fig. 3C are presented as deuterium uptake plots. The values are obtained from the average deuterium uptake levels from all of the amide hydrogens in the indicated regions based on heat maps from three independent experiments. Error bars represent the standard error of three independent experiments. $^{*}p < 0.05$. (For interpretation of the references to colour in this figure legend, the reader is referred to the web version of this article.)

in the basal state β-arrestin2 is more dynamic in β-strands II through IV and is less dynamic in the middle loop than β-arrestin1.

Arrestins interact with more than 30 molecules, but the binding interfaces have not yet been fully mapped [14,15]. The different conformational dynamics between basal state β-arrestin1 and β-arrestin2 may affect the binding characteristics resulting in regulation of different cellular functions. Recent X-ray crystallography and HDX-MS studies provided visualization of the interface between β-arrestin1 and a receptor [25,26]. The X-ray crystallography study revealed several important features of receptor-bound β-arrestin1: (1) the C-tail of β-arrestin1 was displaced, and the C-terminal peptide of a receptor bound to the displaced C-tail empty region; (2) the finger, middle, and lariat loops were rearranged; (3) the N- and C-domains were rotated; and (4) the polar core was disrupted [25]. β-Strands II through IV contain residues that maintain the polar core (e.g. D26 in β-arrestin1 and D27 in β-arrestin2), and therefore the more dynamic feature of β-arrestin2 in these regions might make the polar core more easily disrupted thereby allowing β-arrestin2 to interact with receptors more easily. The HDX-MS study suggested that the three loops (e.g. the finger, middle, and lariat loops) are receptor binding sites [26]. The middle loop (or 139-loop in arrestin1) is especially interesting because it is known to prevent arrestin1 from binding to non-preferred forms of rhodopsin [27]. Therefore, the different conformational dynamics of the middle loop between β-arrestin1 and β-arrestin2 might affect their different receptor selectivities.

3.3. Comparison of conformational dynamics between pre-activated β-arrestin1 and β-arrestin2

Because of their importance in GPCR signaling, the structural mechanism of arrestins has been extensively studied with various techniques including X-ray crystallography, NMR, EPR, and hydrogen/deuterium exchange [13,16–18,25,26,28–33]. These studies

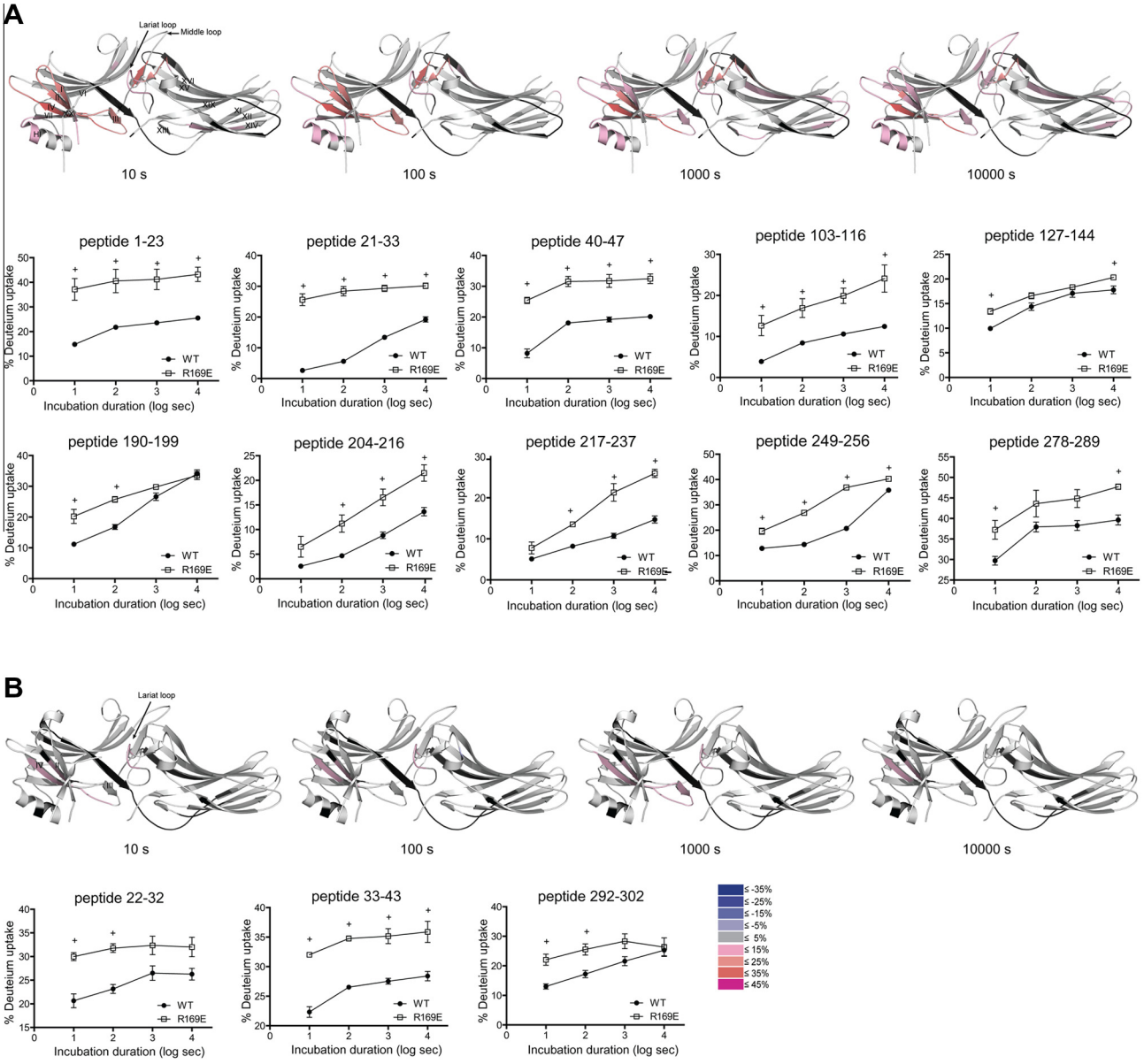

Fig. 4. Conformational changes upon pre-activation. Differential HDX profiles in wild type and R169E mutant were overlaid onto the X-ray crystal structures of β-arrestin1 (A, PDB: 1JSY) and β-arrestin2 (B, PDB: 3P2D). The color legend shows the deuterium uptake difference level. Uncovered regions are in black. Deuterium uptake levels of selected peptic peptides are presented as deuterium uptake plots. Error bars represent the standard error of three independent experiments. $^{*}p < 0.05$. (For interpretation of the references to colour in this figure legend, the reader is referred to the web version of this article.)

have provided insights into the structural mechanism of activation [13,28] and GPCR–arrestin interactions [25,26,29,30]. Previous studies have suggested that two major intramolecular interactions maintain arrestins in the basal conformation [1,34,35] (Fig. 1B); (1) the three-element region connects β-strand I, α-helix I, and β-strand XX in the C-tail [36]; and (2) the polar core, a region composed of solvent-excluded charged residues, maintains the inter-domain interaction mainly by a salt bridge between Arg169 and Asp287 [37]. Elimination of the salt bridge in the polar core by charge reversal (i.e. R169E) has been widely used as a model for pre-activated arrestin, which can interact with GPCRs in a phosphorylation-independent manner [34]. Here, we compared the conformational changes of β-arrestin1 and β-arrestin2 from the basal state (e.g. wild type) to the pre-activated state (e.g. R169E).

To elucidate conformational changes upon pre-activation, deuterium uptake differences between wild type and R169E were visualized as difference heat maps, and the statistical significance of the observed differences is shown as an uptake plot (Fig. 4). β-Arrestin1 underwent statistically higher deuterium uptake in broad regions with the R169E mutation; these regions include β-strands I through IV, α-helix I, β-strand VII, the middle loop, XI/XII loop, β-strands XIII through XVI, and the lariat loop (Fig. 4A). Pre-activation of β-arrestin2 induced statistically increased deuterium uptake in β-strands II through IV and the lariat loop (Fig. 4B). This data revealed that upon pre-activation β-strands II through IV and the lariat loop became more dynamic in both β-arrestin1 and β-arrestin2, whereas β-strand I, α-helix I, β-strand VII, the middle loop, XI/XII loop, and β-strands XIII through XVI became more dynamic only in β-arrestin1 (Fig. 4). To our knowledge, this is the first study to observe these conformational differences between β-arrestin1 and β-arrestin2 upon pre-activation.

Previously, Carter et al. performed a study comparing wild type β-arrestin1 with pre-activated mutants (e.g. R169E and 3A) [13]. Their results were similar to ours; β-strands I through III, near β-strand VII, the middle loop, near β-strand XII, and the lariat loop showed more deuterium uptake in pre-activated mutants than wild type β-arrestin1 [13]. A few regions with changed uptake in our study (e.g. β-strand IV and β-strands XIII through XV) were not changed in the Carter et al. study. These discrepancies may be due to different hydrogen/deuterium exchange, quench, or LC-MS conditions. Recently, Shukla et al. analyzed GPCR-bound β-arrestin1 by HDX-MS [26]. Their results showed that upon GPCR binding deuterium uptake increased in β-strands II through III, β-strand V, and β-strands X through XI, whereas deuterium uptake decreased in the finger, middle, and lariat loops [26]. The authors suggested that the finger, middle, and lariat loops are engaged in the GPCR-β-arrestin1 interface. Interestingly, the N-terminal part (e.g. β-strand II through III) showed increased deuterium uptake levels in our study, the Carter et al. study, and the Shukla et al. study, which implies that the conformational change in this region is a common structural mechanism for β-arrestin activation.

The increased conformational dynamics in β-strand III and the lariat loop that we report here may be due to destabilization of the polar core, because these regions are near amino acid residues that form the polar core (e.g. D26 and D287 in β-arrestin1 and D27 and D289 in β-arrestin2). This conformational change may propagate to neighboring regions such as β-strand II and IV, which also became more dynamic in both β-arrestin1 and β-arrestin2. The regions that became more dynamic only in β-arrestin1 (e.g. β-strand I, α-helix I, β-strand VII, the middle loop, XI/XII loop, and β-strands XIII through XVI) may determine the differential cellular functions between β-arrestin1 and β-arrestin2. β-Strands V through VI and β-strands XV through XVI in arrestin1 and β-arrestin1 were reported to play key roles in receptor preference [38]. Therefore, the differential conformational change between β-arrestin1 and β-arrestin2 in β-strands XV through XVI may reflect different receptor selectivities. The differential conformational change between β-arrestin1 and β-arrestin2 would also affect differential binding capacities for other cellular molecules such as JNK3 [14,15]. However, because of the lack of a precise binding interface map of arrestin and interacting molecules, it is not easy to clearly define the functional differences created by these structural differences. Therefore, defining an interface map of arrestin with interacting molecules is of great interest for furthering our understanding of the structural mechanism of arrestin functions.

Acknowledgments

This work was supported by the basic science research program (NRF-2012R1A1A1039220), the medical research center program (NRF-2012R1A5A2A28671860) of the National Research Foundation of Korea, and the Samsung Research Fund, Sungkyunkwan University, 2012.

References

[1] M.J. Lohse, C. Hoffmann, Arrestin interactions with G protein-coupled receptors, Handb. Exp. Pharmacol. 219 (2014) 15–56.
[2] H. Kuhn, S.W. Hall, U. Wilden, Light-induced binding of 48-kDa protein to photoreceptor membranes is highly enhanced by phosphorylation of rhodopsin, FEBS Lett. 176 (1984) 473–478.
[3] M.J. Lohse, J.L. Benovic, J. Codina, M.G. Caron, R.J. Lefkowitz, Beta-Arrestin: a protein that regulates beta-adrenergic receptor function, Science 248 (1990) 1547–1550.
[4] H. Attramadal, J.L. Arriza, C. Aoki, T.M. Dawson, J. Codina, M.M. Kwatra, S.H. Snyder, M.G. Caron, R.J. Lefkowitz, Beta-arrestin2, a novel member of the arrestin/beta-arrestin gene family, J. Biol. Chem. 267 (1992) 17882–17890.
[5] S.S. Ferguson, W.E. Downey 3rd, A.M. Colapietro, L.S. Barak, L. Menard, M.G. Caron, Role of beta-arrestin in mediating agonist-promoted G protein-coupled receptor internalization, Science 271 (1996) 363–366.
[6] O.B. Goodman Jr., J.G. Krupnick, F. Santini, V.V. Gurevich, R.B. Penn, A.W. Gagnon, J.H. Keen, J.L. Benovic, Beta-arrestin acts as a clathrin adaptor in endocytosis of the beta2-adrenergic receptor, Nature 383 (1996) 447–450.
[7] T.A. Kohout, F.S. Lin, S.J. Perry, D.A. Conner, R.J. Lefkowitz, Beta-Arrestin 1 and 2 differentially regulate heptahelical receptor signaling and trafficking, Proc. Natl. Acad. Sci. U.S.A. 98 (2001) 1601–1606.
[8] R.H. Oakley, S.A. Laporte, J.A. Holt, M.G. Caron, L.S. Barak, Differential affinities of visual arrestin, beta arrestin1, and beta arrestin2 for G protein-coupled receptors delineate two major classes of receptors, J. Biol. Chem. 275 (2000) 17201–17210.
[9] A. Tohgo, E.W. Choy, D. Gesty-Palmer, K.L. Pierce, S. Laporte, R.H. Oakley, M.G. Caron, R.J. Lefkowitz, L.M. Luttrell, The stability of the G protein-coupled receptor-beta-arrestin interaction determines the mechanism and functional consequence of ERK activation, J. Biol. Chem. 278 (2003) 6258–6267.
[10] T.J. Povsic, T.A. Kohout, R.J. Lefkowitz, Beta-arrestin1 mediates insulin-like growth factor 1 (IGF-1) activation of phosphatidylinositol 3-kinase (PI3K) and anti-apoptosis, J. Biol. Chem. 278 (2003) 51334–51339.
[11] M. Schumann, T. Nakagawa, S.A. Mantey, B. Howell, R.T. Jensen, Function of non-visual arrestins in signaling and endocytosis of the gastrin-releasing peptide receptor (GRP receptor), Biochem. Pharmacol. 75 (2008) 1170–1185.
[12] W.E. Miller, P.H. McDonald, S.F. Cai, M.E. Field, R.J. Davis, R.J. Lefkowitz, Identification of a motif in the carboxyl terminus of beta-arrestin2 responsible for activation of JNK3, J. Biol. Chem. 276 (2001) 27770–27777.
[13] J.M. Carter, V.V. Gurevich, E.R. Prossnitz, J.R. Engen, Conformational differences between arrestin2 and pre-activated mutants as revealed by hydrogen exchange mass spectrometry, J. Mol. Biol. 351 (2005) 865–878.
[14] V.V. Gurevich, E.V. Gurevich, W.M. Cleghorn, Arrestins as multi-functional signaling adaptors, Handb. Exp. Pharmacol. (2008) 15–37.
[15] E.V. Gurevich, V.V. Gurevich, Arrestins: ubiquitous regulators of cellular signaling pathways, Genome Biol. 7 (2006) 236.
[16] M. Han, V.V. Gurevich, S.A. Vishnivetskiy, P.B. Sigler, C. Schubert, Crystal structure of beta-arrestin at 1.9 A: possible mechanism of receptor binding and membrane translocation, Structure 9 (2001) 869–880.
[17] X. Zhan, L.E. Gimenez, V.V. Gurevich, B.W. Spiller, Crystal structure of arrestin-3 reveals the basis of the difference in receptor binding between two non-visual subtypes, J. Mol. Biol. 406 (2011) 467–478.
[18] Y. Zhuo, S.A. Vishnivetskiy, X. Zhan, V.V. Gurevich, C.S. Klug, Identification of receptor binding-induced conformational changes in non-visual arrestins, J. Biol. Chem. 289 (2014) 20991–21002.
[19] K.N. Nobles, Z. Guan, K. Xiao, T.G. Oas, R.J. Lefkowitz, The active conformation of beta-arrestin1: direct evidence for the phosphate sensor in the N-domain and conformational differences in the active states of beta-arrestins1 and -2, J. Biol. Chem. 282 (2007) 21370–21381.

[20] M.P. Gray-Keller, P.B. Detwiler, J.L. Benovic, V.V. Gurevich, Arrestin with a single amino acid substitution quenches light-activated rhodopsin in a phosphorylation-independent fashion, Biochemistry 36 (1997) 7058–7063.
[21] V.V. Gurevich, J.L. Benovic, Mechanism of phosphorylation-recognition by visual arrestin and the transition of arrestin into a high affinity binding state, Mol. Pharmacol. 51 (1997) 161–169.
[22] S.R. Marcsisin, J.R. Engen, Hydrogen exchange mass spectrometry: what is it and what can it tell us?, Anal Bioanal. Chem. 397 (2010) 967–972.
[23] Y. Bai, J.S. Milne, L. Mayne, S.W. Englander, Primary structure effects on peptide group hydrogen exchange, Proteins 17 (1993) 75–86.
[24] G.P. Connelly, Y. Bai, M.F. Jeng, S.W. Englander, Isotope effects in peptide group hydrogen exchange, Proteins 17 (1993) 87–92.
[25] A.K. Shukla, A. Manglik, A.C. Kruse, K. Xiao, R.I. Reis, W.C. Tseng, D.P. Staus, D. Hilger, S. Uysal, L.Y. Huang, M. Paduch, P. Tripathi-Shukla, A. Koide, S. Koide, W.I. Weis, A.A. Kossiakoff, B.K. Kobilka, R.J. Lefkowitz, Structure of active beta-arrestin-1 bound to a G-protein-coupled receptor phosphopeptide, Nature 497 (2013) 137–141.
[26] A.K. Shukla, G.H. Westfield, K. Xiao, R.I. Reis, L.Y. Huang, P. Tripathi-Shukla, J. Qian, S. Li, A. Blanc, A.N. Oleskie, A.M. Dosey, M. Su, C.R. Liang, L.L. Gu, J.M. Shan, X. Chen, R. Hanna, M. Choi, X.J. Yao, B.U. Klink, A.W. Kahsai, S.S. Sidhu, S. Koide, P.A. Penczek, A.A. Kossiakoff, V.L. Woods Jr., B.K. Kobilka, G. Skiniotis, R.J. Lefkowitz, Visualization of arrestin recruitment by a G-protein-coupled receptor, Nature 512 (2014) 218–222.
[27] S.A. Vishnivetskiy, F. Baameur, K.R. Findley, V.V. Gurevich, Critical role of the central 139-loop in stability and binding selectivity of arrestin-1, J. Biol. Chem. 288 (2013) 11741–11750.
[28] Y.J. Kim, K.P. Hofmann, O.P. Ernst, P. Scheerer, H.W. Choe, M.E. Sommer, Crystal structure of pre-activated arrestin p44, Nature 497 (2013) 142–146.
[29] T. Zhuang, Q. Chen, M.K. Cho, S.A. Vishnivetskiy, T.M. Iverson, V.V. Gurevich, C.R. Sanders, Involvement of distinct arrestin-1 elements in binding to different functional forms of rhodopsin, Proc. Natl. Acad. Sci. U.S.A. 110 (2013) 942–947.
[30] M. Kim, S.A. Vishnivetskiy, N. Van Eps, N.S. Alexander, W.M. Cleghorn, X. Zhan, S.M. Hanson, T. Morizumi, O.P. Ernst, J. Meiler, V.V. Gurevich, W.L. Hubbell, Conformation of receptor-bound visual arrestin, Proc. Natl. Acad. Sci. U.S.A. 109 (2012) 18407–18412.
[31] S.K. Milano, H.C. Pace, Y.M. Kim, C. Brenner, J.L. Benovic, Scaffolding functions of arrestin-2 revealed by crystal structure and mutagenesis, Biochemistry 41 (2002) 3321–3328.
[32] J.A. Hirsch, C. Schubert, V.V. Gurevich, P.B. Sigler, The 2.8 A crystal structure of visual arrestin: a model for arrestin's regulation, Cell 97 (1999) 257–269.
[33] J. Granzin, U. Wilden, H.W. Choe, J. Labahn, B. Krafft, G. Buldt, X-ray crystal structure of arrestin from bovine rod outer segments, Nature 391 (1998) 918–921.
[34] V.V. Gurevich, X. Song, S.A. Vishnivetskiy, E.V. Gurevich, Enhanced phosphorylation-independent arrestins and gene therapy, Handb. Exp. Pharmacol. 219 (2014) 133–152.
[35] V.V. Gurevich, E.V. Gurevich, Structural determinants of arrestin functions, Prog. Mol. Biol. Transl. Sci. 118 (2013) 57–92.
[36] S.A. Vishnivetskiy, C. Schubert, G.C. Climaco, Y.V. Gurevich, M.G. Velez, V.V. Gurevich, An additional phosphate-binding element in arrestin molecule. Implications for the mechanism of arrestin activation, J. Biol. Chem. 275 (2000) 41049–41057.
[37] S.A. Vishnivetskiy, C.L. Paz, C. Schubert, J.A. Hirsch, P.B. Sigler, V.V. Gurevich, How does arrestin respond to the phosphorylated state of rhodopsin?, J Biol. Chem. 274 (1999) 11451–11454.
[38] S.A. Vishnivetskiy, M.M. Hosey, J.L. Benovic, V.V. Gurevich, Mapping the arrestin-receptor interface. Structural elements responsible for receptor specificity of arrestin proteins, J. Biol. Chem. 279 (2004) 1262–1268.